Electronic Structure of Ni Substituted $Y(Ni_{1-x}M_x)_2B_2C$ Superconductors

Z. Zeng[a], *D.E. Ellis*[b], *Diana Guenzburger*[a] *and E. M. Baggio-Saitovitch*[a]

[a]Centro Brasileiro de Pesquisas Físicas - CBPF
Rua Dr. Xavier Sigaud, 150
22290-180 Rio de Janeiro, RJ, Brasil

[b]Department of Physics and Astronomy and Materials Research Center,
Northwestern University, Evanston, IL 60208, U.S.A.

ABSTRACT

The substitution of Ni by the transition metals Fe, Co and Ru in YNi_2B_2C is analyzed using the self-consistent local density embedded-cluster approach. Changes of partial densities of states, charge density, and bond order are examined to elucidate bonding structure and the interplay between covalent, ionic, and metallic interactions in these highly anisotropic superconductors. Impurity induced modifications in distribution and composition of states near the Fermi level are discussed in terms of the observed drop in T_c with impurity concentration. Electric field gradients are obtained at the central site. In the case of iron substitution with concentration $x \leq 0.1$, electric quadrupole splitting is compared with Mössbauer experimental results.

PACS 74.70.-b

Key-words: Quaternary superconductors; Electronic structure; Borocarbides.

1 Introduction

A number of quaternary intermetallic borocarbides RM_2B_2C (R=rare earth, M=transition metal) are superconductors with T_c as high as 23K (YPd_2B_2C)[1-5]. This superconducting phase has a highly anisotropic structure which is a variant of the layered $ThCr_2Si_2$-type structure[3,4] with an additional carbon in the R plane. Electronic band structure calculations for RNi_2B_2C (R=Y, Lu) [6-9] using density functional theory revealed that states around the Fermi level are dominated by nickel, which leads to a metallic phase with Ni-Ni distance somewhat shorter than in the pure metal. Thus the role played by transition metal sites in RM_2B_2C compounds in both transport and superconducting properties is dominant, and is reflected in the simplest model in terms of the Ni partial density of states (PDOS) at the Fermi energy. Thus it is important to understand how the metallic structure is maintained in the RNi_2B_2C crystal, and how it is modified by substitution , defects, *etc.* Substitution of Ni by its neighbors in the periodic table such as Fe, Co and the isoelectronic 4d elements (Pd, Ru, Rh) provide a supposedly mild "perturbation", which can be used to study the important metal-metal interactions both experimentally and theoretically.

The complete substitution of Ni by Pd, Pt, or Co in the same crystal phase as YNi_2B_2C has been reported[5,10,11]; notably, $T_c \rightarrow 0$ in YCo_2B_2C. Table 1 shows how T_c varies with element substitution in YM_2B_2C (M=Ni, Pt, Pd, Co) systems. The partial substitutions of Ni in YNi_2B_2C by Co, Fe and Ru performed by Bud'ko *et al.*[12a] and A. K. Gangopadhyay *et al.*[13] induced a linear decrease of T_c with impurity concentration. Table 1 also gives values of T_c for these partial substitutions [12a]. The experimental measurements show that the metal substitutions for the same concentration decrease T_c of the pure compound in the order: Ru > Fe > Co > Pd. The observed decrease of T_c could be interpreted as a shift of the Fermi level with respect to the Ni peak in the DOS. While a rigid band model is probably oversimplified, it provides an attractive explanation in terms of net 3d band occupancy, which can be tested by several techniques. Moreover, hyperfine interactions have also been studied at Fe and Co sites using ^{57}Fe Mössbauer[12b] and ^{59}Co NMR measurements[14]. These studies provide information about the probe-atom electronic charge and spin densities through the electric field gradient(EFG) and the effective magnetic hyperfine field.

Following these experimental works, we study here the electronic structure of $Y(Ni_{1-x}M_x)_2B_2C$ (M=Fe, Co, Ru; x=0.07, 0.47) using the first-principles density functional embedded-cluster approach. We also analyze the electronic structure and bonding of the pure species YNi_2B_2C, which will provide a theoretical background for comparisons with the impurity systems. We obtain information about changes in the densities of states, the variation of charge transfer and local atomic configurations due to the various substituents. Electric field gradients are obtained at the metal site, and in the case of iron substitution, comparison is made with experiment.

2 Theoretical Method and Cluster Model

The discrete variational (DV) embedded-cluster approach is used throughout this work, in the framework of density functional theory[15]. The effective atomic configurations of the cluster atoms are obtained self-consistently by iterating the charge and spin density, using the von Barth-Hedin exchange and correlation potential [16] and a least-squares fit of model parameters to the eigenvector densities[17]. The embedding scheme treats interactions between the variational cluster and the infinitely extended host crystal[18]. This is accomplished by embedding the cluster in the charge density of several shells of atoms of the external part of the crystal, with charges approximately equal to those in the cluster. The Madelung potential is included by employing Ewald summations.

Local properties such as hyperfine interactions are obtained from the electronic density,

$$\rho(\vec{r}) = \sum_k n_k |\phi_k(\vec{r})|^2 \tag{1}$$

where n_k are the occupation numbers which are chosen for the ground state according to Fermi-Dirac statistics, and $\phi_k(\vec{r})$ are the cluster orbitals. The cluster orbitals are expanded as a linear combination of numerical symmetrized atomic orbitals. The variational method leads to the secular equations, which are solved self-consistently in a 3-dimensional numerical grid[19]. A Mulliken-type population analysis is performed to obtain atomic orbital populations and atomic charges[19]. Partial densities of states (DOS) are defined by [19b]:

$$D^q_{nl\sigma}(\varepsilon) = \sum_i P^q_{nl\sigma,i} \frac{\delta/\pi}{(\varepsilon - \varepsilon_{i\sigma})^2 + \delta^2} \tag{2}$$

where $P^q_{nl\sigma,i}$ is the Mulliken population of atomic orbital χ_{nl} of atom q in the cluster spin orbital $\phi_{i\sigma}$, and δ is the half-width of the Loretzian functions employed to broaden the cluster levels, to simulate a continuum ($\delta = 0.136eV$ here). By summing over n, l and i the local DOS of spin σ for atom q is obtained.

The electric quadrupole splitting (ΔEQ) is proportional to the electric field gradient V_{zz}, which for the 14.4keV transition of ^{57}Fe is given by:

$$\Delta EQ = \frac{eV_{zz}}{2} Q (1 + \frac{\eta^2}{3})^{1/2} \tag{3}$$

Here Q is the ^{57}Fe nuclear quadrupole moment and η is the asymmetry parameter, which is zero in axial symmetry. Estimated values of Q range from 0.08b to 0.41b [20]; more frequently employed values are in the range of 0.15-0.21b.

The electric field gradient is determined by three parts:

(1) The valence electron matrix element (in atomic units):

$$V^{val}_{zz} = - < \rho(3z^2 - r^2)/r^5 >; \tag{4}$$

(2) the contribution from nuclei and core electrons of the local cluster:

$$V^{nuc}_{zz} = \sum_{\nu}^{cluster} Q_\nu (3z^2_\nu - r^2_\nu)/r^5_\nu; \tag{5}$$

Where Q_ν is the charge of the ionic core at site ν (atomic number minus number of core electrons).

(3) Contributions of host ions V_{zz}^{host}, which has a similar expression to Eq. (4) with effective total net charge q_ν. In the present calculations, these were not considered, since the values are small (<10% of total) due to the denominator as was verified in other cluster calculations for ionic solids[21].

The variational cluster (shown in Fig. 1) used to simulate $Y(Ni_{1-x}M_x)_2B_2C$ has 71 atoms and composition $Y_{12}(Ni,M)_{15}B_{32}C_{12}$ with D_{2d} symmetry. M represents the substitution element Fe, Co or Ru, with concentration x. We chose two concentrations, 0.07 and 0.47, to simulate the dilute impurity and a near 50-50 substitution composition while keeping the cluster symmetry unchanged. When analyzing local properties such as partial densities of states and magnetic moments, the atom at the center of the cluster is preferably chosen, since all its bonding capacity is satisfied, as it is in the bulk. Therefore, the substituted compounds always have one M atom at the center in their cluster representation. The numerical atomic basis orbitals include 4s, 4p, 4d, 5s, 5p of Y, 3s, 3p, 3d, 4s, 4p of the transition element, and 1s, 2s, 2p of B and C. The deep-lying atomic orbitals were treated in the frozen-core approximation, *i.e.*, were assumed to not change from the free atom values. The valence basis was explicitly orthogonalized against the core. The B and C 1s orbitals were treated as valence orbitals due to the strong covalency between boron and carbon as evidenced by the short bond length. The crystal structure and interatomic distances of YNi_2B_2C were taken from references [1b,3,4]; for the substituted compounds, the distances were considered unchanged.

3 Results and Discussion

A. Densities of States

The DOS of the parent compound YNi_2B_2C is shown in Fig. 2. The PDOS shows that the dominant features near ε_F are due to Ni (the transition metal more generally). However, significant contributions are visible from B, due to metal-B covalency, and also a weak "tail" of diffuse yttrium valence states due to its interaction with C. The carbon contributions to $N(\varepsilon_F)$ are small. The cluster PDOS are thus entirely consistent with band structure results for YNi_2B_2C[6-9], although of lower resolution due to cluster size effects. In particular, we note that ε_F falls on a subpeak III of the DOS (Fig. 2), which has been identified as a critical feature for the relatively high T_c of YNi_2B_2C. The nature of states forming this peak is analyzed in more detail below.

We have analyzed the cluster eigenvalues distribution around the Fermi level; the DOS subpeak III corresponds to 5 closely spaced levels. The atomic orbital contributions from Ni 3d, B 2p, C 2p and Y 4d5s5p to these levels are shown in Table 2. In addition to the predominant contribution from Ni 3d, those from B 2p and C 2p are also noticeable as can also be seen in the PDOS curves (Fig. 2). The weak "tail" of Y spd states is small (3-13%) but cannot be ignored, since it will play a strong role in transport in the c-axis direction.

The strong covalency between boron and carbon is evident in the strong overlap be-

tween their PDOS. Figure 2 displays three peaks in the B and C PDOS around -0.98Ry, -0.7Ry, and -0.36Ry. The first peak at -0.98 Ry corresponds mainly to C 2s, with some mixture with B. The second peak at -0.7Ry is constituted mainly of C $2p_z$, which bonds with B. The third peak at ∼-0.36Ry in the C PDOS corresponds to C ($2p_x$, $2p_y$), which forms bonds with Y on the Y-C plane. This last peak in the B PDOS has a significant overlap with the Ni PDOS, representing the strong B s-p hybrid involved in Ni-B bonding. Similar structures also appear in the Fe, Co and Ru substitution cases.

With a net 3d occupation of 9.06 (Table 3) the main Ni 3d peaks (I, II) are located well below the Fermi level, which also has significant Ni 4p character, according to Figs. 2 and 3. The secondary peak III near the Fermi level, which also has significant Ni 4p character, is shifted and broadened with the substitution by Fe, Co and Ru, as seen in Fig. 4.

In the pure compound YNi_2B_2C, Ni is a weak electron donor, with a net charge of 0.16 on the average. When its metal neighbors are substituted by atoms such as Fe, Co and Ru with fewer d electrons (-2, -1 and -2), a rigid band model would predict a shift of ε_F to the low-energy side of the Ni 3d PDOS peak. However, as we see from Fig. 4 and Tables 3-5, the net 3d population of Ni is not reduced, instead its PDOS is somewhat broadened, and reduced in amplitude by dilution with Fe, Co or Ru. As can be seen from Fig. 5, the substituent d PDOS are substantially different from Ni. The secondary peak III is seen to lie well above ε_F in both Fe and Co, as would be expected. Thus substitution by Fe and Co will lower the total density of states at ε_F and consequently reduce T_c. Details of structure near ε_F and in the occupied region depend noticeably on concentration. For example, dilute Fe and Co (x=0.07) show relatively sharp features which can be associated with ligand-field splittings of the atomic 3d levels, and a low-energy metal-B covalent band tail. At higher concentration (x=0.47) both Fe and Co 3d structures become more diffuse and begin to resemble the (shifted) Ni 3d PDOS. At all concentrations, the Ru 4d PDOS appears as a broad diffuse band, consisting of a strong low energy (-0.4Ry) Ru-B bonding component, a three-peak "conduction band" region, and a weak feature at ε_F which is linked to Ni 3d states. Finally, the Ru "secondary peak" appears at 0.08∼0.1Ry above ε_F, rising in energy with concentration. Thus Ru substitution should have a similar effect of reducing DOS(ε_F) and thus T_c.

B. Self-consistent Atomic Configurations

The calculated shift and broadening in the Ni 3d PDOS with the substitution of Fe, Co and Ru can be attributed in part to hybridization between Ni and the substituent, and in part to lattice disorder induced by substitution, which leads to multiple inequivalent Ni sites. A semiquantitative picture of M-Ni charge transfer can be obtained from the Mulliken populations of Tables 3-5. In these tables, the net charges were obtained by also taking into account the variational 3s, 3p populations of the first-row transition metals and 4s, 4p of Y and Ru (not included in the Table). These "shallow core" populations are slightly reduced with respect to the free atom values, and are known to have important (shielding) effects on hyperfine properties.

Thus we see that Ni has a net charge of +0.16 (the center site has 0.11, due to its

special symmetry) in the pure compound, initially losing about 0.01 3d electrons under Fe substitution, see Table 3. At the same time, the net charge on the nearest neighbor boron is changed by -0.01 or +0.03, depending on Fe concentration. The Fe net charge varies from +0.06 (x=0.07) to -0.04 (x=0.47) primarily due to changes in diffuse 4s4p occupancy.

Using the one-electron energy band model other workers have emphasized the correlation between $D(\varepsilon_F)$, the density of states at the Fermi energy, and T_c. This quantity enters as an exponential factor in the theory of conventional superconductors. Here we point out an equally strong correlation with the integrated partial density of states, or net metal 3d population (see Eq.2):

$$N_d = \int_{-\infty}^{\varepsilon_F} D_d(\varepsilon) d\varepsilon \tag{6}$$

This quantity also enters in the usual theories of pair-wise electron correlations, which are essential in the formation of the superconducting state.

For a system of composition $A_{1-x}B_x$, we could represent both total DOS and orbital populations as

$$N_{nl}^{AB} = (1-x)N_{nl}^{A} + xN_{nl}^{B} \tag{7}$$

Here N^A, N^B are occupancy of nl atomic orbitals in system A and B. In a rigid-band scheme, N_{nl}^A and N_{nl}^B are as in the pure metals A and B. If we consider $Ni_{1-x}Fe_x$ with 3d band occupancies of ~9 and ~7 for Ni and Fe, respectively, estimated from pure metal band structure calculations, an improved rigid-band model for the Fe-substituted compound will give:

$$\widetilde{N}_{3d} = 9(1-x) + 7x + N_{3d}^0 \tag{8}$$

where N_{3d}^0 is a hybridization term due to mixing with ligands (*e.g.*, Ni-B). Analogous expressions may be constructed for the other substitutional transition metals.

The population data on Tables 3-5 permit a direct test of this rigid-band model. In fact, we may calculate directly the weighted average N_d populations using the Ni and M self-consistent d populations given in Tables 3-5 for each substituted compound, for x=0.07 and x=0.47, employing Eq. 7. On the other hand, we may also calculate $\widetilde{N}_d$ with Eq. 8 (the hybridization term N_d^0 is obtained by making x=0 and equating $N_d = \widetilde{N}_d$). Both N_d and $\widetilde{N}_d$ are presented in Tables 3-5. Comparing the rigid-band parameter $\widetilde{N}_d$ with the self-consistent N_d, we see that this simple rigid-band model gives a rather accurate result for $\widetilde{N}_d$ at low concentration (x=0.07), but deviates significantly at higher doping levels. For values of x=0.07, relevant to the experimental data of Table 1, both N_d and $\widetilde{N}_d$ correlate well with T_c, as shown in Fig. 6.

The populations and net charges for $Y(Ni_{1-x}Co_x)_2B_2C$ (Table 4) show almost identical Ni response to substitution by Co as by Fe. Of course, the substituent charges and populations ($Fe^{+0.06}3d^{7.28}$ versus $Co^{+0.05}3d^{8.23}$ for x=0.07) are quite different, and characteristic of their relative position in the periodic table. Iron and ruthenium are isoelectronic; however, the Ru 4d function is more extended than Fe 3d. The chemical state of Ru reflects the more diffuse 4d character, with charge and population $Ru^{+0.10}4d^{7.48}$ versus $Fe^{+0.06}3d^{7.28}$ for x=0.07, for example (see Table 5). The Ni response to doping in the two cases is quite similar, *e.g.* $Ni^{+0.17}3d^{9.10}$ for $Fe_{0.07}$ versus $Ni^{+0.16}3d^{9.10}$ for $Ru_{0.07}$.

However, referring again to the band structure results, we observe that changes of less than 0.1 in occupancy in the Ni 3d PDOS are sufficient to move ε_F significantly relative to the sharp peak, and thus alter T_c. A linear fit to the T_c *vs.* N_d data gives a "sensitivity" $dT_c/dN_d = 68K/electron$.

The atomic orbital populations show that yttrium is highly ionic in all cases with charge 2.47-2.49. Deviation from "ideal" Y^{3+} character is primarily due to occupancy of the 4d shell (*e.g.* $4d^{0.54}5s^{0.06}5p^{0.05}$ in YNi_2B_2C) which contributes weakly but significantly to the structure of the DOS (see Fig. 2) around ε_F. These states are doubtlessly essential to conduction in the c-axis direction. The boron populations show a strong s-p hybridization, with net charge ~-0.35 marking the strong TM-B covalency in tetrahedral coordination. The typical charge associated with carbon is ~-1.75 and can be interpreted most simply in terms of ionic charge transfer from Y in the YC "rock-salt" slab [1].

C. Charge Distribution and Bonding

Table 6 gives the bond orders (shared charge) [22] between nearest neighbors in $Y(Ni_{1-x}M_x)_2B_2C$, which give a measure of the degree of bonding between atoms. Positive bond orders indicate a bond between atoms; negative bond orders indicate that the atoms repel each other (antibonding interaction).

The bonding between boron and carbon (1.14) in the pure YNi_2B_2C compound is the strongest component, as may be expected. Substitution of a small amount of Ni by Fe, Co or Ru decreases this bonding by 1-4%, showing that the more extended wave functions of Fe, Co and Ru affect the B-C bonding strength. The anti-bonding, mainly ionic interaction between Y and C with bond order -0.18 practically doesn't change with TM substitution, showing that this interaction is strongly localized in the Y-C slab. The Ni-B bond order of ~0.64 is quite stable, but weakened somewhat (3%) with Ru substitution. The M-B substituent bond orders are larger than those of the host Ni-B. It would be interesting to compare this with the corresponding pure compounds, taking into account experimental lattice constants.

The extremely strong covalent bonding between B and C can best be seen in charge density contour maps, presented below.

Fig. 7a shows the charge density $\rho(\vec{r})$ in the Ni plane (x-y plane) of the pure YNi_2B_2C system. We see that, with the Ni-Ni distance compressed to less than that of bulk Ni (2.45Å vs 2.50Å of fcc Ni), the metal atoms have a noticeable charge accumulation along bond lines. A transverse view (y-z plane, Fig. 7b) shows a Ni layer coupled covalently to the rigid B-C-B columns lying along the c-axis. In the lower part of the figure, one can see the somewhat aspherical Y ions of the YC layer.

The difference charge density between the compound YNi_2B_2C (P) and $Y(Ni_{0.93}Fe_{0.07})_2B_2C$ (IP), $\Delta\rho = \rho(IP) - \rho(P)$, are presented in figure 8. Solid lines represent positive $\Delta\rho$, dashed lines represent $\Delta\rho < 0$; the center of the diagram is nickel or iron (note the use of multiple contour intervals to make bond features apparent). Apparently, nickel atoms around the Fe (substitution) site give up some charge transferred to the substituent while the second neighbors also have $\Delta\rho > 0$. Table 3 show that the net charge transfer on these sites is quite small. Thus graphical methods are essential for understanding the

subtle charge rearrangements which takes place under TM substitution.

Looking in the y-z plane (Fig. 8b) we see there is a very little charge transfer between boron and the substitution site, with a small shift of charge from C towards B. The strong covalency between B and C is indifferent to any charge transfer as well as rearrangement within the metal plane. Similarly, we note only an extremely weak charge accumulation on the Y site; the Y ionic state is determined essentially by its coordination to C and is unresponsive to metal-plane substitutions. These conclusions, based on direct examination of $\Delta\rho$, verify the general picture obtained from populations and bond orders, discussed above.

D. Electric field gradients

Electric field gradients originate from the asphericity of the charge distribution around the probe atom. Table 7 gives the values of the electric field gradients at the metal atom placed at the center of the cluster, calculated according to Eqs. 4 and 5. It is seen that the magnitude of the total V_{zz} is very small for Ni and the Fe substituent, larger for Co, and much larger for Ru. The predicted signs of V_{zz} are negative for Fe and Co, and positive for Ni and Ru. This change of sign is due to the positive valence electrons contribution V_{zz}^{val} for Ni and Ru substitution being larger than the negative V_{zz}^{nuc}.

Electric field gradients in transition metals arise from the charge asphericity of the (primarily) d and p electrons[23],[24]. For the present substituted compounds, the positive values of V_{zz}^{val} obtained in all cases indicated that the contributions in the (x,y) (transition metal) plane due to $d_{x^2-y^2}$, d_{xy} and p_x, p_y, which are positive, dominate over those with components in the z axis (d_{z^2}, d_{xz}, d_{yz} and p_z), which are negative.

It must be kept in mind that all distances were considered equal to those in YNi_2B_2C. Calculations for the interatomic distances as in the substituted compounds could show differences from the present values, since V_{zz} is a sensitive quantity due to the factor r^{-3}. However, since the atomic radii of Fe, Co and Ni are very similar, distances should be significantly different only for Ru, whose atomic radius is ~5% larger.

We may notice from Table 7 that there is little difference in V_{zz}, for each probe metal, between x=0.07 and x=0.47. This is due to fact that only metal atoms second-neighbor to the central atom were replaced when changing from x=0.07 to x=0.47. This result is evidence of the very local nature of field gradients, which is due to the r^3 denominator in the matrix elements.

In Table 7 is given the experimental electric quadrupole splitting for Fe, obtained by Mössbauer spectroscopy of the substituted compound with less than 10%Fe[14]. Considering the small magnitude of ΔEQ, the accord between theory and experiment may be considered good. To obtain V_{zz} for the Ru substituent, Mössbauer spectroscopy of ^{99}Ru could be utilized; for Cobalt, NMR experiments have been made but the resolution of the spectrum did not allow to determine the quadrupole interaction so far[14].

4 Conclusions

We have performed Density Functional calculations for 71-atom clusters representing the quaternary substituted superconductor compounds $Y(Ni_{1-x}M_x)_2B_2C$. The partial DOS analysis leads to an understanding of the drop in T_c, which is observed experimentally[12], by substitution with M=Fe, Co, Ru in terms of the net number of alloy d-electrons. The rigid-band model was found to be entirely inadequate to describe the changes in DOS around the Fermi level, which are crucial in the understanding of superconductivity only for low-doping concentration. Mulliken populations, bond orders and charge density maps gave a description of the electronic charge distribution in the pure and substituted crystal. Our results show that the strong B-C covalent bonding and essentially ionic Y-C bonding structure are insensitive to substitution in the TM plane. Electric field gradients were calculated for all cases; the positive values obtained for V_{zz} of the valence electrons are related to the dominant contribution from electrons in the (x,y) (transition metal) plane.

Acknowledgments

Calculations were performed at the Cray YMP of the Supercomputing Center of the Universidade Federal do Rio Grande do Sul. This work was supported by RHAE-New Material Project no. 610195/92-1 and that of D.E. Ellis in part by the U.S. National Science Foundation, through the Materials Research Center at Northwestern University, Grant no.DMR-9120521. The authors thank Luiz Marcelo Oliveira for the computer figure of the cluster. Stimulating discussions with S.L. Bud'ko and M. El Massalami are acknowledged.

FIGURE CAPTIONS

*Fig.*1. The $Y_{12}(Ni,M)_{15}B_{32}C_{12}$ cluster model simulating $Y(Ni_{1-x}M_x)_2B_2C$ (M=Fe, Co and Ru) compounds.

*Fig.*2. The total and partial DOS of YNi_2B_2C compound. Energies are relative to Fermi energy. The unit cell has two molecular units.

*Fig.*3. Individual orbital PDOS of Ni for YNi_2B_2C.

*Fig.*4. Ni 3d PDOS in $Y(Ni_{1-x}M_x)_2B_2C$ for M=Fe, Co and Ru.

*Fig.*5. Substituents d PDOS in $Y(Ni_{1-x}M_x)_2B_2C$ for M=Fe, Co and Ru.

*Fig.*6. Plot of T_c versus N_d for $YNi_{1-x}M_xB_2C$. N_d calculated according to Eq. 7, using the self-consistent populations. Values of N_d for x=0.03 and x=0.05 were obtained by linear interpolation between x=0.0 and x=0.07.

*Fig.*7. Contour plots of charge density of YNi_2B_2C in (a) (110) plane (Ni atoms only) with contour range [0,0.06] with interval 0.01, [0.07,0.2] with interval 0.04 and [0.3,1.0] with interval 0.3; (b) (011) plane (see Fig. 1), with contour range [0.0,0.1] with interval of 0.01 (in e/a_0^3).

*Fig.*8. A typical contour plot of the difference charge density between the doped and the pure compounds: ($Y(Ni_{0.93}Fe_{0.07})_2B_2C$ - YNi_2B_2C) along a) (110)plane and b) (011) plane with the contour range [-0.5,-0.1] with interval 0.02, [-0.1,-0.01] with interval 0.04 and [-0.01,0.01] with interval 0.001 (in e/a_0^3).

TABLE CAPTIONS

Table **1.** The superconducting transition temperature T_c in Yttrium based systems. (a) from reference [1b], (b) from reference [10], (c) from reference [5], (d) from reference [13] and (e) from reference [12].

Table **2.** Atomic orbital populations (in % of one electron) for specific cluster eigenvalues around the Fermi level. Energies are given with respect to ε_F. Contributions less than 5% were not considered.

Table **3.** Mulliken atomic orbital populations for YNi_2B_2C and $Y(Ni_{1-x}Fe_x)_2B_2C$. Ni_c represents the Ni atom at the cluster center site, and Ni represents an average over Ni-occupied sites, not including the center. Values for Fe are for the Fe atom at the center. The column "charge" is the net charge on each atom. 3s, 3p orbitals of the transition metal, as well as 4s, 4p of Y, not included in the table, show small deviations of their populations with respect to the free atom values. N_d and $\widetilde{N}_d$ are defined in the text (see Eqs. 7 and 8).

Table **4.** Mulliken atomic orbital populations for $Y(Ni_{1-x}Co_x)_2B_2C$ with the same entry meaning as in Table 3. Values for Co are for the Co atom at the center.

Table **5.** Mulliken atomic orbital populations for $Y(Ni_{1-x}Ru_x)_2B_2C$. Values for Ru are for the Ru atom at the center.

Table **6.** The bond order between component atoms in $Y(Ni_{1-x}M_x)_2B_2C$ (M=Fe, Co and Ru) compounds. In the case of the pure compound, M=Ni represents cluster central atom which is the substitution site.

Table **7.** Components (Eqs. 3 and 4) and total electric field gradients V_{zz} for $Y(Ni_{1-x}M_x)_2B_2C$, calculated for M at the central position in the cluster. Theoretical values of ΔEQ for Fe were obtained with $Q(^{57}Fe)$=0.21b. The sign of ΔEQ was not obtained experimentally.

a) From ref. [12b].

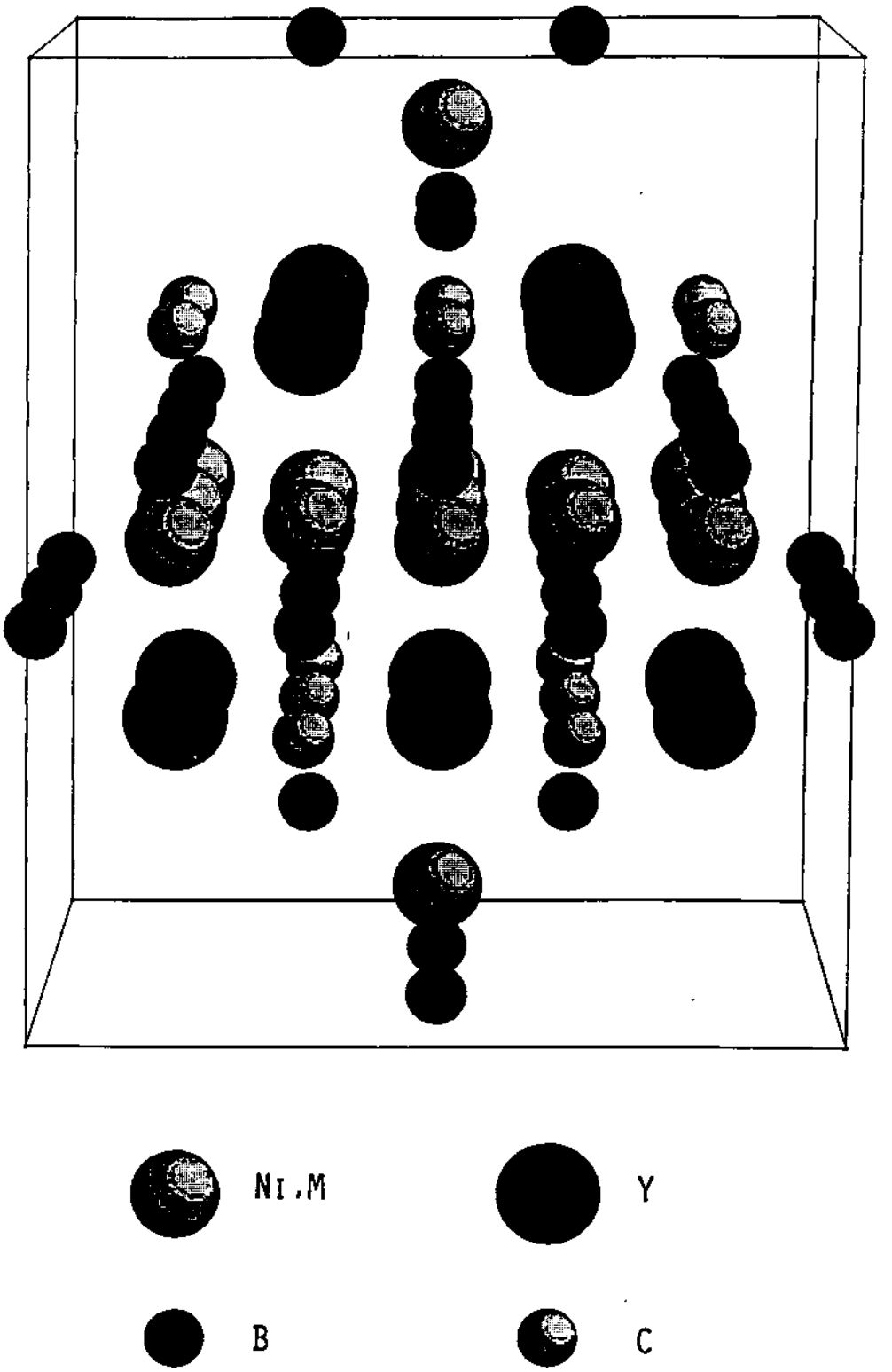

Fig. 1

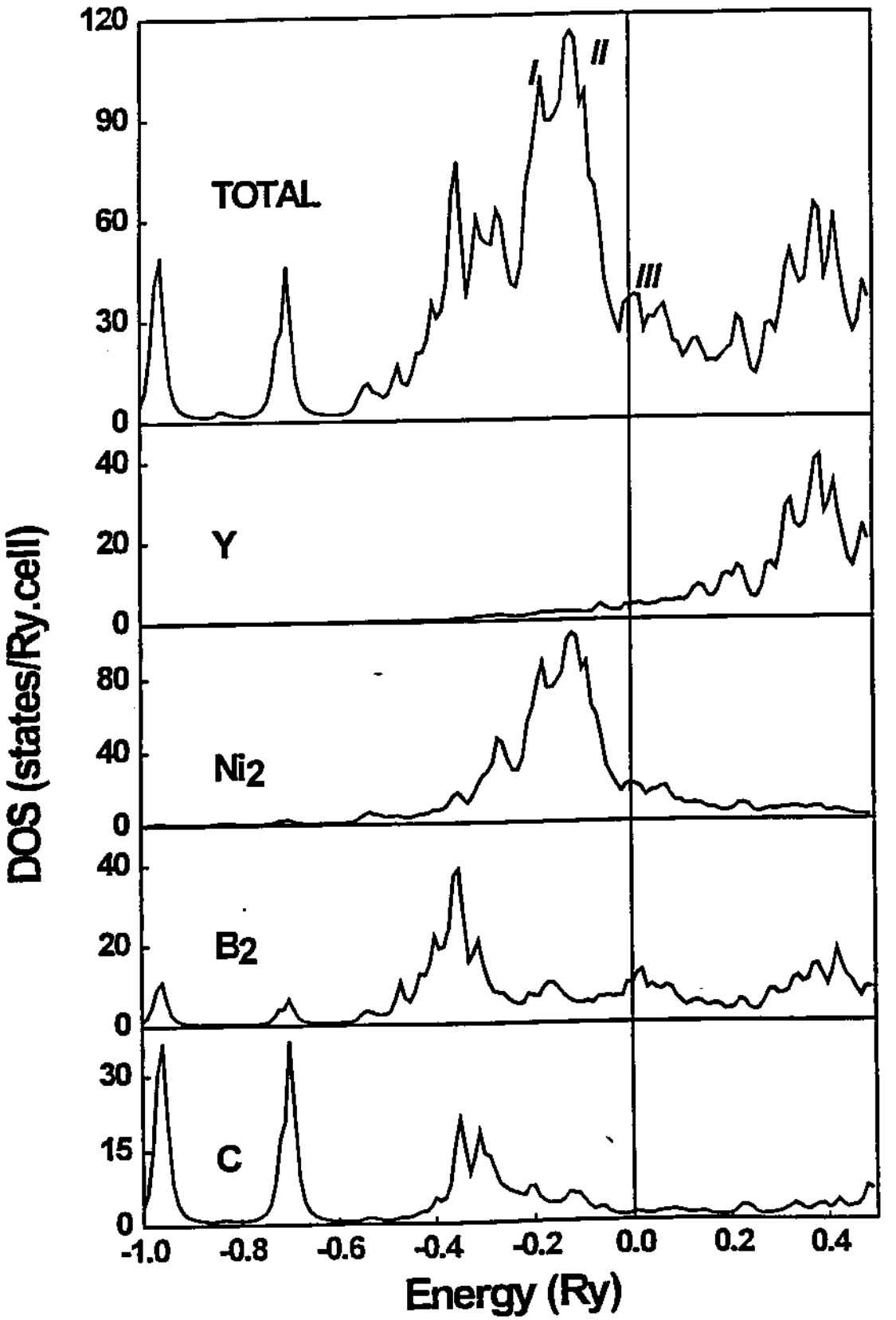
120
90
60
30
0
TOTAL
I
II
III
40
20
0
Y
80
40
0
Ni2
40
20
0
B2
30
15
0
C
-1.0
-0.8
-0.6
-0.4
-0.2
0.0
0.2
0.4
Energy (Ry)
DOS (states/Ry.cell)

Fig. 2

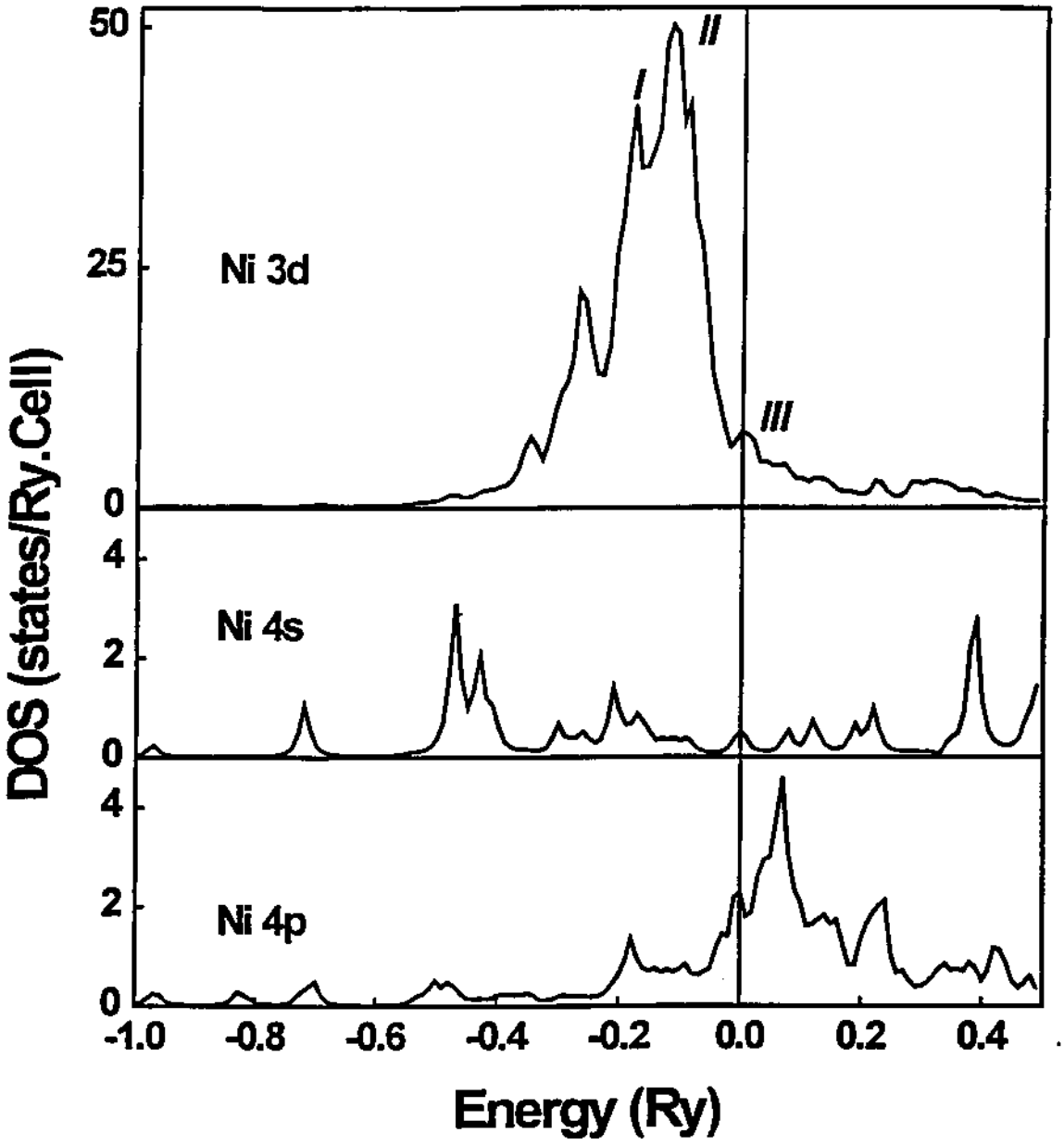
50
25
0
Ni 3d
I
II
III
4
2
0
Ni 4s
4
2
0
Ni 4p
-1.0
-0.8
-0.6
-0.4
-0.2
0.0
0.2
0.4
DOS (states/Ry.Cell)
Energy (Ry)

Fig. 3

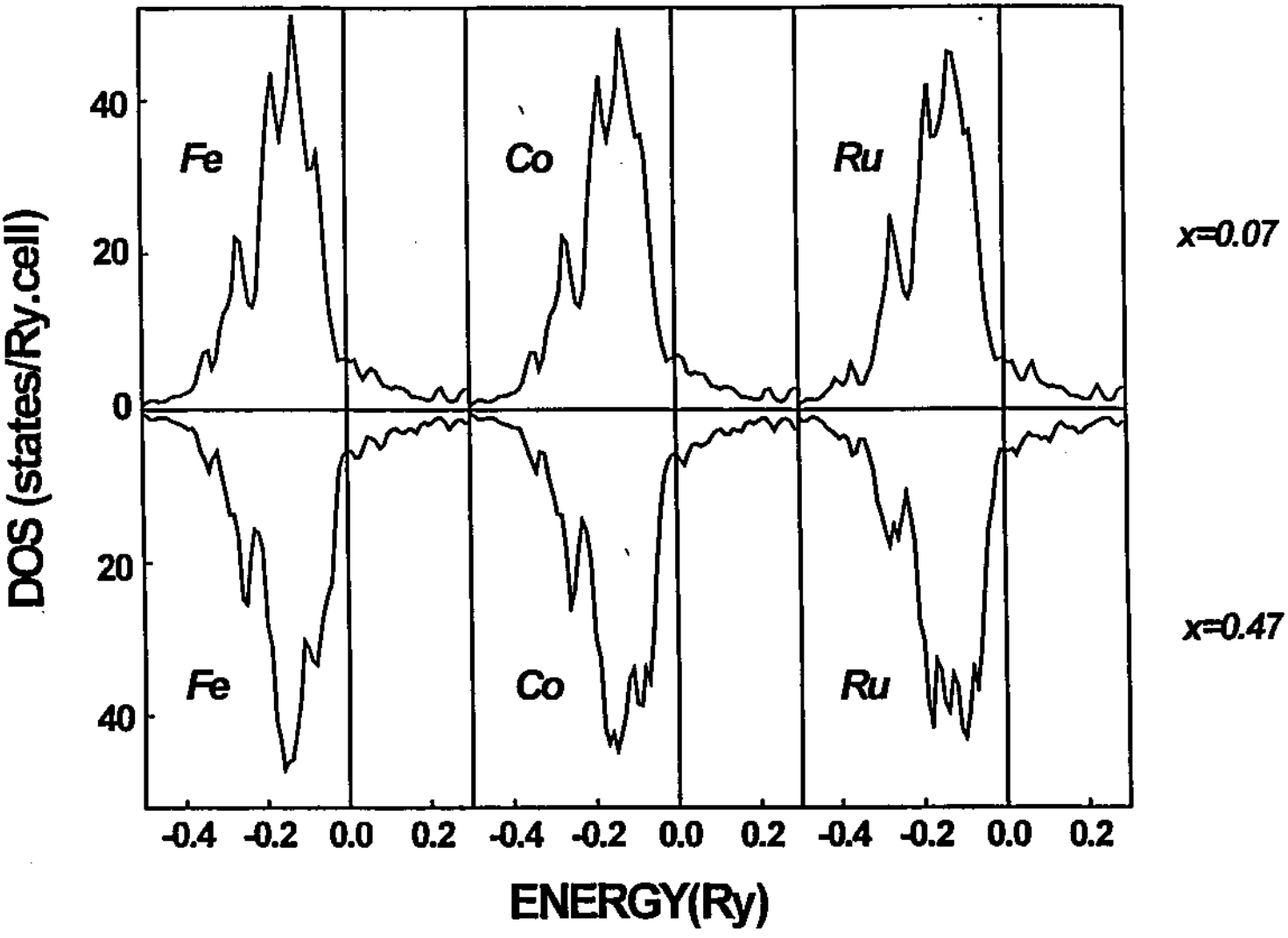
DOS (states/Ry.cell)
40
20
0
20
40
Fe
Co
Ru
Fe
Co
Ru
x=0.07
x=0.47
-0.4
-0.2
0.0
0.2
ENERGY(Ry)

Fig. 4

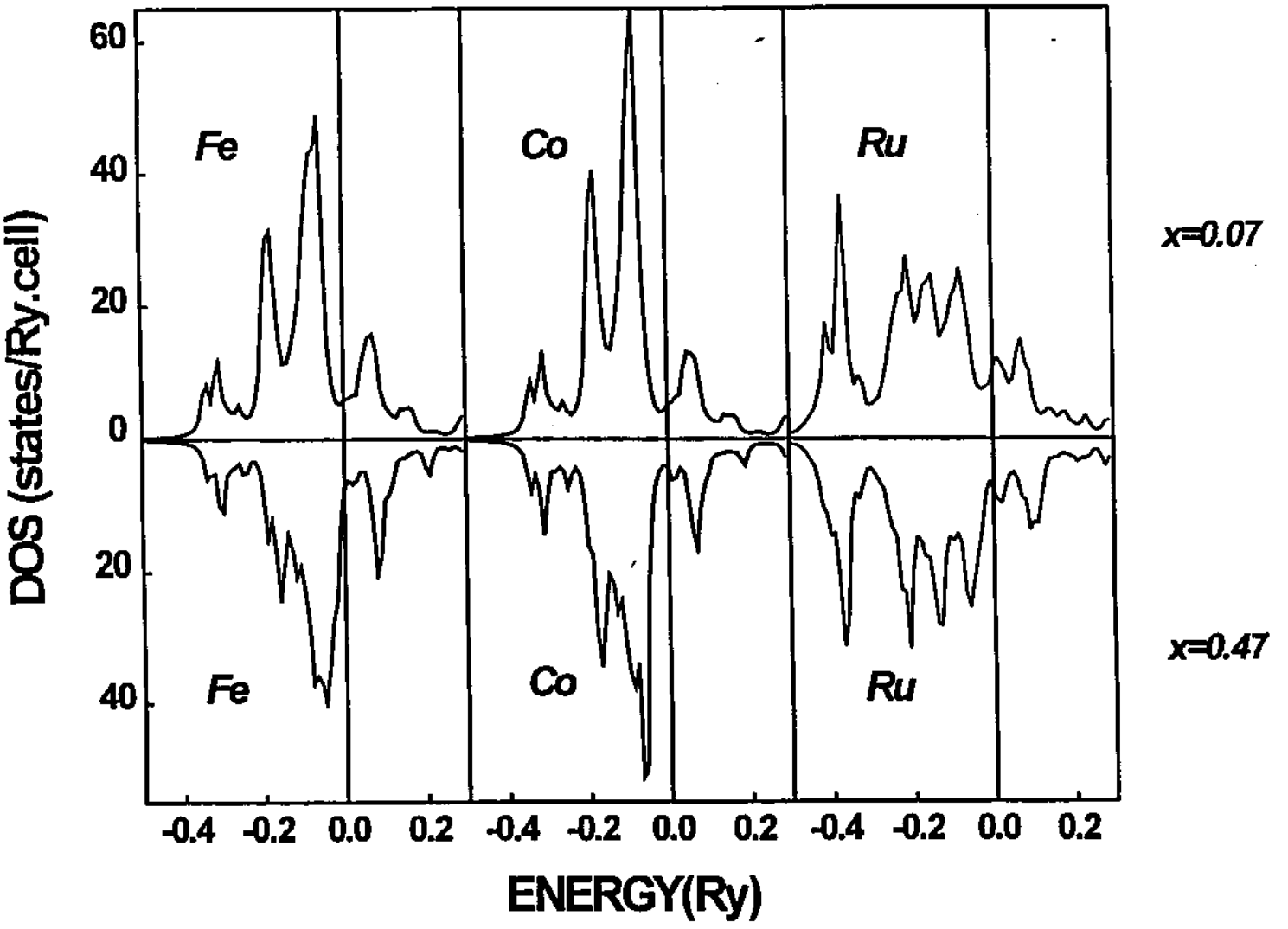
DOS (states/Ry.cell)
60
40
20
0
20
40
Fe
Co
Ru
x=0.07
x=0.47
-0.4
-0.2
0.0
0.2
ENERGY(Ry)

Fig. 5

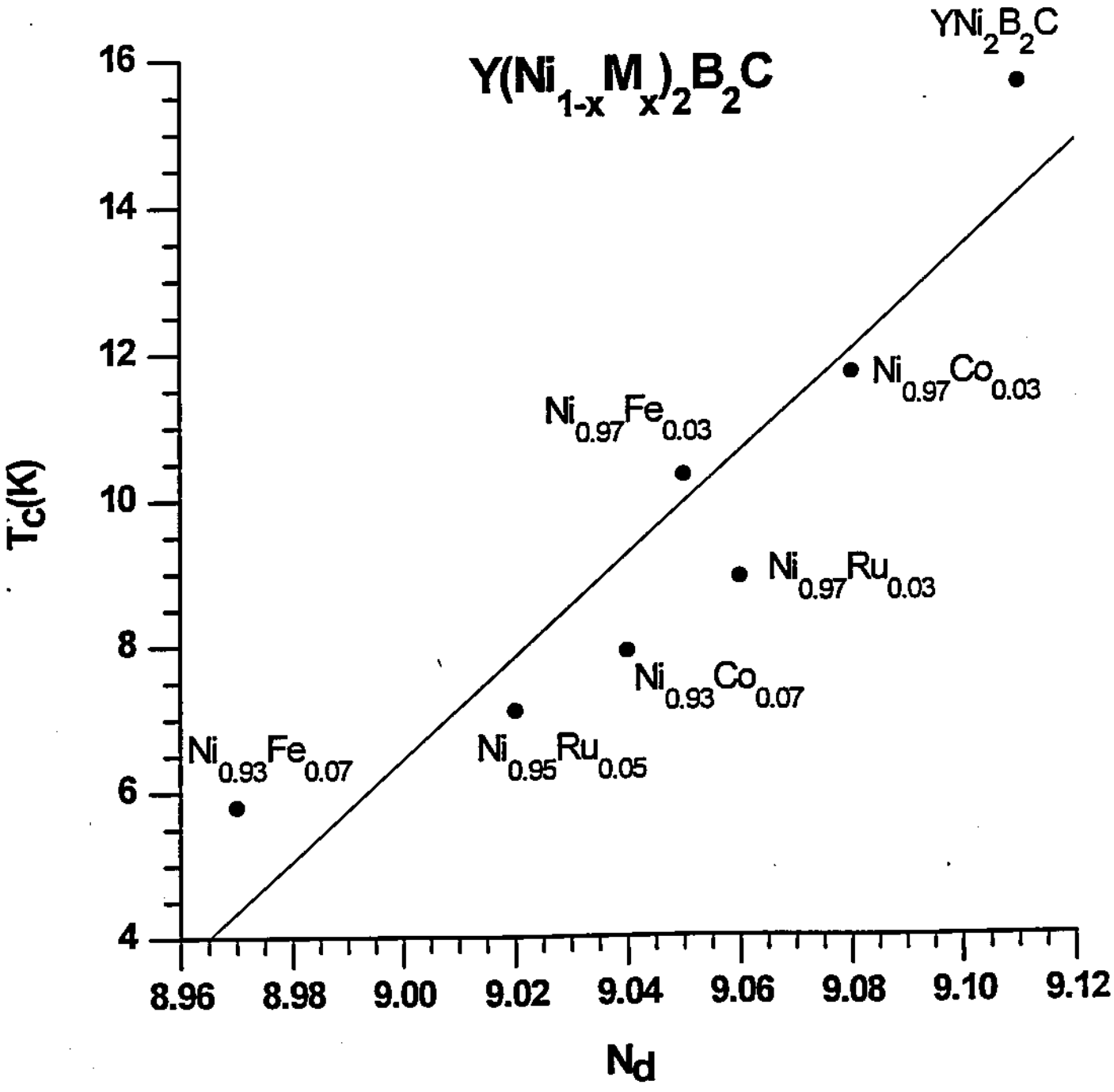
Y(Ni1-xMx)2B2C
YNi2B2C
Ni0.97Co0.03
Ni0.97Fe0.03
Ni0.97Ru0.03
Ni0.93Co0.07
Ni0.95Ru0.05
Ni0.93Fe0.07
Tc(K)
Nd
16
14
12
10
8
6
4
8.96
8.98
9.00
9.02
9.04
9.06
9.08
9.10
9.12

Fig. 6

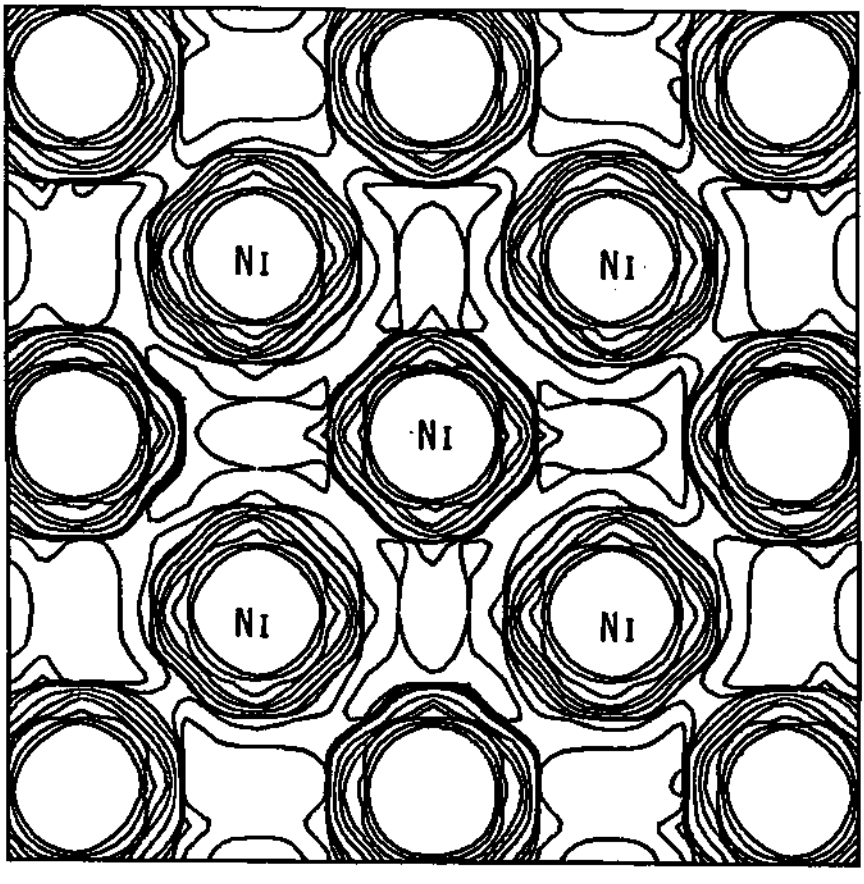

Fig. 7a

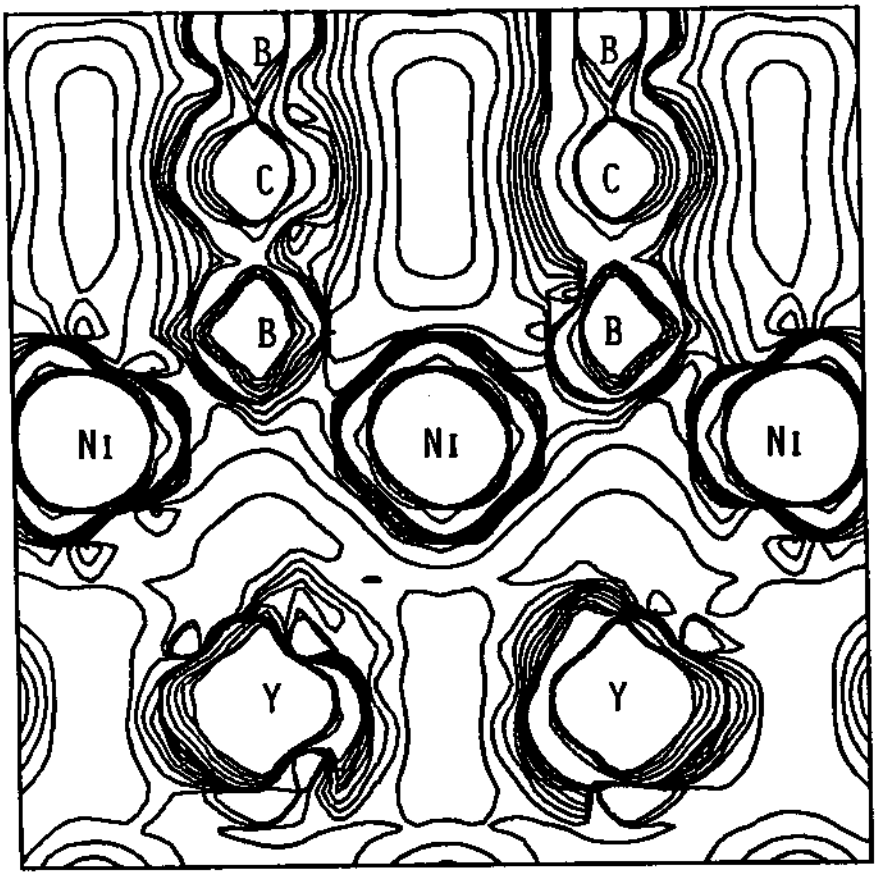

Fig. 7b

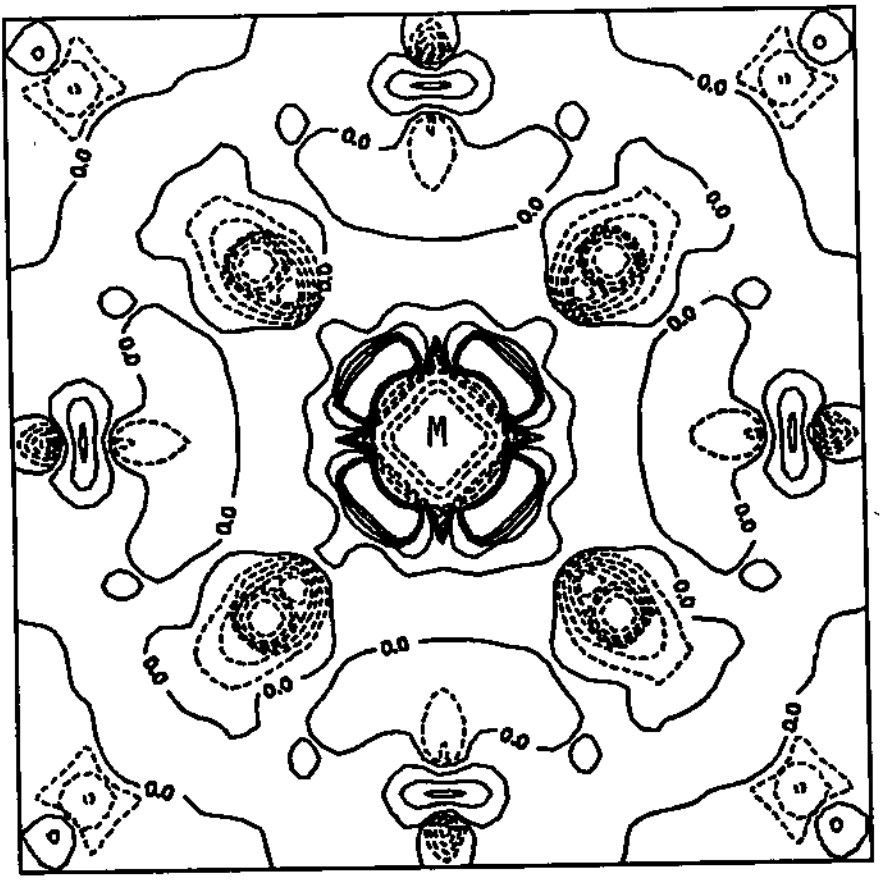

Fig. 8a

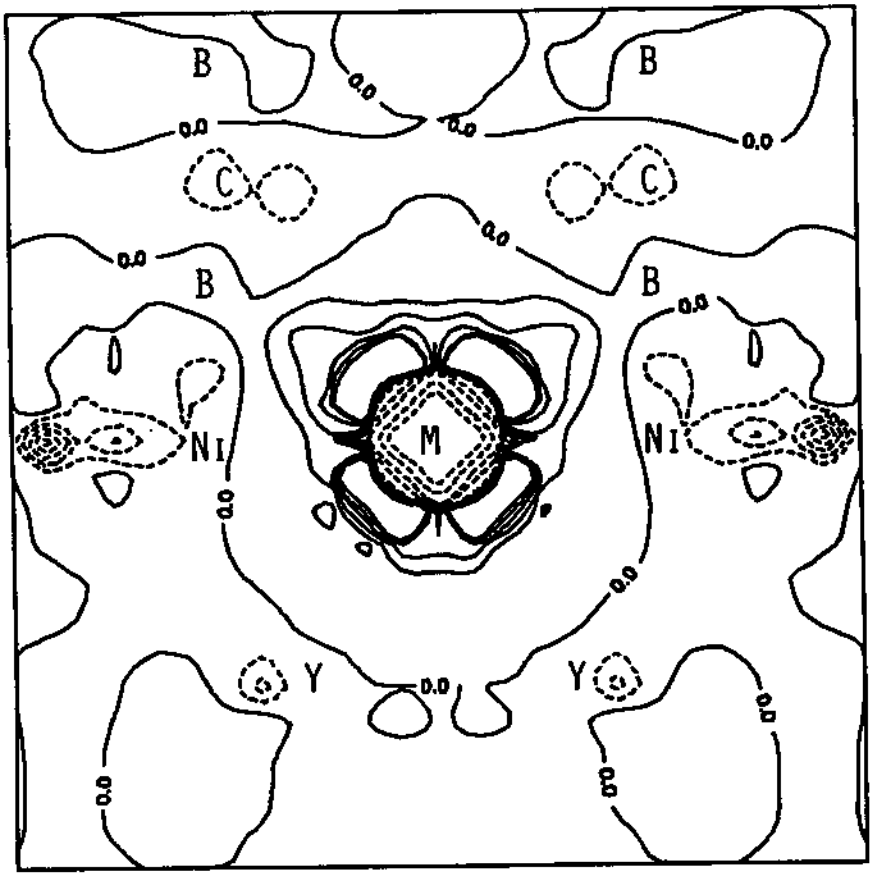

Fig. 8b

Table 1

YNi_2B_2C	15.6K [a]
YPt_2B_2C	10.0K [b]
YPd_2B_2C	23.0K [c]
YCo_2B_2C	0.0K [d]
$Y(Ni_{0.97}Fe_{0.03})_2B_2C$	10.3K [e]
$Y(Ni_{0.93}Fe_{0.07})_2B_2C$	5.8K [e]
$Y(Ni_{0.97}Co_{0.03})_2B_2C$	11.7K [e]
$Y(Ni_{0.93}Co_{0.07})_2B_2C$	7.9K [e]
$Y(Ni_{0.97}Ru_{0.03})_2B_2C$	8.9K [e]
$Y(Ni_{0.95}Ru_{0.05})_2B_2C$	7.1K [e]

Table 2

Energy (Ry.)	Atomic orbital population			
	Ni 3d	B 2p	C 2p	Y 4d5s5p
+0.0038	50%	17%	12%	13%
-0.0014	44%	18%	25%	9%
-0.0062	63%	21%	3%	10%
-0.0092	41%	40%	11%	3%
-0.0102	41%	18%	34%	3%

Table 3

YNi_2B_2C					$Y(Ni_{1-x}Fe_x)_2B_2C$								
	x=0.00					x=0.07				0.47			
Ni_c	3d	4s	4p	charge	Fe	3d	4s	4p	charge	3d	4s	4p	charge
	9.06	0.38	0.52	0.11		7.28	0.31	0.45	0.06	7.35	0.30	0.41	-0.04
B	2s	2p			B	2s	2p			2s	2p		
	0.82	2.53		-0.35		0.81	2.55		-0.36	0.80	2.52		-0.32
Ni	3d	4s	4p		Ni	3d	4s	4p		3d	4s	4p	
	9.11	0.41	0.39	0.16		9.10	0.41	0.39	0.17	9.11	0.42	0.38	0.16
Y	4d	5s	5p		Y	4d	5s	5p		4d	5s	5p	
	0.54	0.06	0.05	2.49		0.54	0.06	0.05	2.49	0.54	0.06	0.05	2.48
C	2s	2p			C	2s	2p			2s	2p		
	1.40	4.35		-1.75		1.40	4.34		-1.74	1.40	4.36		-1.76
N_d	9.11					8.97				8.28			
$N_{\bar{d}}$	9.11					8.97				8.17			

Table 4

	x=0.07				0.47			
Co	3d	4s	4p	charge	3d	4s	4p	charge
	8.23	0.33	0.46	0.05	8.24	0.33	0.49	0.02
B	2s	2p			2s	2p		
	0.81	2.53		-0.34	0.81	2.52		-0.33
Ni	3d	4s	4p		3d	4s	4p	
	9.10	0.41	0.39	0.17	9.10	0.42	0.38	0.16
Y	4d	5s	5p		4d	5s	5p	
	0.54	0.06	0.05	2.49	0.54	0.06	0.05	2.49
C	2s	2p			2s	2p		
	1.40	4.35		-1.75	1.39	4.36		-1.75
N_d	9.04				8.70			
$\tilde{N}_d$	9.04				8.64			

Table 5

	x=0.07				0.47			
Ru	4d	5s	5p	charge	4d	5s	5p	charge
	7.48	0.25	0.43	0.10	7.50	0.24	0.38	0.12
B	2s	2p			2s	2p		
	0.78	2.57		-0.36	0.75	2.60		-0.34
Ni	3d	4s	4p		3d	4s	4p	
	9.10	0.41	0.40	0.16	9.07	0.43	0.45	0.13
Y	4d	5s	5p		4d	5s	5p	
	0.55	0.07	0.05	2.48	0.56	0.07	0.06	2.47
C	2s	2p			2s	2p		
	1.40	4.34		-1.74	1.39	4.35		-1.74
N_d	8.99				8.33			
$\tilde{N}_d$	8.97				8.17			

Table 6

	YNi_2B_2C	$Y(Ni_{1-x}Fe_x)_2B_2C$		$Y(Ni_{1-x}Co_x)_2B_2C$		$Y(Ni_{1-x}Ru_x)_2B_2C$	
x	0.00	0.07	0.47	0.07	0.47	0.07	0.47
Ni-B	0.64	0.64	0.62	0.64	0.64	0.62	0.62
Y-C	-0.18	-0.18	-0.18	-0.18	-0.18	-0.18	-0.17
B-C	1.14	1.12	1.13	1.13	1.13	1.09	1.12
M-B	0.66	0.72	0.72	0.68	0.69	0.68	0.67

Table 7

M	$V_{zz}^{val.}(e/a_0^3)$	$V_{zz}^{nuc.}(e/a_0^3)$	$V_{zz}(e/a_0^3)$	$V_{zz}(10^{17}V/cm^2)$	calculated ΔEQ(mm/s)	experiment ΔEQ(mm/s)
Ni, x=0.00	0.74	-0.65	0.09	+0.87	–	–
Fe, x=0.07	0.61	-0.65	-0.04	-0.39	-0.09	$\|0.18\|\pm0.04^{(a)}$
Fe, x=0.47	0.50	-0.63	-0.13	-1.26	-0.26	–
Co, x=0.07	0.28	-0.65	-0.37	-3.59	–	–
Co, x=0.47	0.24	-0.64	-0.40	-3.89	–	–
Ru, x=0.07	1.96	-0.65	1.31	+12.7	–	–
Ru, x=0.47	1.95	-0.63	1.32	+12.8	–	–

REFERENCES

1. a) R.J. Cava, H. Takagi, B. Batlogg, H. W. Zandbergen, J.J. Krajewski, W.F. Peck Jr., R.B. van Dover, R.J. Felder, T. Siegrist, K. Mizuhashi, J.O. Lee, H. Eisaki, S.A. Carter, S. Uchida, Nature, **367**, 146(1994).

   b) R.J. Cava, H. Takagi, H.W. Zandbergen, J.J. Krajewski, W.F. Peek Jr., T. Siegrist, B. Batlogg, R.B. van Dover, R.J. Felder, K. Mizuhashi, J.O. Lee, H. Eisaki and S. Uchida, Nature, **367**, 252(1994).

2. R. Nagarajan, C. Mazumdar, Z. Hossain, S.K. Dhar, K.V. Gopalakrishnan, L.C. Gupta, C. Godart, B.D. Padalia and R. Vijayaraghavan, Phys. Rev. Lett. **72**, 274(1994).

3. T. Siegrist, H. W. Zandbergen, R.J. Cava, J.J. Krajewski and W.F. Peck Jr., Nature **367**, 254(1994).

4. H.W. Zandbergen, R.J. Cava, J.J. Krajewski, W.F. Peck Jr., Physica C **224**, 6(1994).

5. Y. Y. Sun, I. Rusakova, R. L. Meng, Y. Cao, P. Gautier-Picard and C. W. Chu, Physica C, **230**, 435(1994).

6. W. E. Pickett and D. J. Singh, Phys. Rev. Lett. **72**, 3702(1994).

7. L.F. Mattheiss, Phy. Rev. B, **49**, 13279(1994).

8. R. Coehoorn, Physica C, **228**, 331(1994).

9. J.I. Lee, T.S. Zhao, I.G. Kim, B.I. Min and S.J. Youn, Phys. Rev. B, **50**, 4030(1994)

10. R.J. Cava, B. Batlogg, T. Siegrist, J.J. Krajewski, W.F. Peck Jr., S. Carter, R.J. Felder, H. Takagi and R.B. van Dover, Phys. Rev. B**49**, 12384(1994).

11. H. Schmidt, M. Müller and H.F. Braun, Proceedings of the International Conference on Materials and Mechanisms of Superconductivity of High Temperature Superconductors (1994).

12. a) S.L. Bud'ko, M. El Massalami, M.B. Fontes, J. Mondragon, W. Vanoni, B. Giordanengo and E. M. Baggio-Saitovitch, Physica C, **243**, 183(1995);

    b) E. M. Baggio-Saitovitch, M.B. Fontes and S.L. Bud'ko, Latin-American Conference on Mössbauer Spectroscopy, Chile (1994).

13. A. K. Gangopadhyay, A. J. Schuetz and J. S. Schilling, Physica C, **246**, 317(1995).

14. S.L. Bud'ko, M.B. Fontes, D. Aliaga-Guerra and E.M.B. Saitovitch, accepted for publication in Phy. Rev. B.

15. D.E. Ellis, Int. J. Quant. Chem. Suppl. **2**, 35(1968); D.E. Ellis and G.S. Painter, Phys. Rev. B, **2**, 2887(1970).

16. U. von Barth and L. Hedin, J. Phys. C, **5**, 1629(1972).

17. B. Delley and D.E. Ellis, J. Chem. Phys, **76**, 1949(1982).

18. D.E. Ellis, G.A. Benesh and E. Byrom, Phys. Rev. B, **16**, 3308(1977).

19. a) D.E. Ellis, J. Guo and J.J. Low, in "Quantum Chemistry Approached to Chemisorption and Heterogeneous Catalysis", ed. F. Ruette, Kluwer, Amsterdam(1992).

    b) P.L. Cao, D.E. Ellis and A.J. Freeman, Phys. Rev. B, **25**, 2124(1982).

20. N.N. Greenwood and T.C. Gibb, "Mössbauer Spectroscopy", Champman and Hall, London(1971); K.J. Duff, K.S. Mishra and T.P. Das, Phys. Rev. Lett. **46**, 1611(1981).

21. J. Terra and D. Guenzburger, Phys. Rev. B, **44**, 8584(1991).

22. A. Szabo, "Modern Quantum Chemistry", McMillan, N. York(1982), p.138.

23. D. Guenzburger and D.E. Ellis, Phys. Rev. B, **36**, 6971(1987).

24. D. Guenzburger and D.E. Ellis, Phys. Rev. B, **22**, 4203(1980).